INSTITUTE FOR FUSION STUDIES

DOE/ET/53088-440 IFSR #440

Vlasov-Maxwell Equilibria of Solar Coronal Loops

V. Krishan and *T. D. Sreedharan*
Indian Institute of Astrophysics
Bangalore 560034, India

and

Swadesh M. Mahajan
Institute for Fusion Studies
The University of Texas at Austin
Austin, Texas 78712

July 1990

THE UNIVERSITY OF TEXAS

AUSTIN

Vlasov-Maxwell Equilibria of Solar Coronal Loops

V. KRISHAN and T. D. SREEDHARAN
Indian Institute of Astrophysics
Bangalore 560034, India
and
SWADESH M. MAHAJAN
Institute for Fusion Studies
The University of Texas at Austin
Austin, Texas 78712

Summary

A Vlasov-Maxwell description of the ubiquitous solar Coronal structures is presented. It is found that an equilibrium plasma configuration can live with spatial gradients in density, temperature, current, and drift speeds of the charged particles. Any stability study must be carried over this inhomogeneous equilibrium state. In addition, the Vlasov description admits the investigation of kinetic processes like heating and radiation.

1. Introduction

Solar coronal loops have been conventionally studied through magnetohydrodynamic processes since their shapes betray the underlying magnetic fields. Coronal loops are especially favored for their ability to pick up energy from the convection zone and deposit it in the corona. The foot points of the loops suffer continuous turning and twisting, producing complex magnetic geometry in which current sheets have been shown to form by many. One believes that ohmic dissipation of current in these sheets can maintain a million degree corona. Attempts to show the formation of extremely small scale current sheets constitute the efforts of Parker (1983, 1987), Low (1987), Low and Wolfson (1988), Ballegoovijen (1985, 1986), Karpen et al. (1990), and many more. The MHD equilibria of coronal loops have been investigated by Priest (1981), Hood and Priest (1979), Vaiana et al. (1978), Tsinganos (1982), Krishan (1983, 1985), and Krishan, Berger, and Priest (1988). In this paper, we explore a Vlasov-Maxwell treatment of a current carrying cylindrical plasma. In this description, it is possible to derive the spatial profiles of equilibrium plasma parameters as well as the exact particle velocity distribution functions. It is found that the system develops strongly peaked current density profiles under very commonly occurring conditions. It is perhaps the disturbance of these current density configurations that leads to the heating and acceleration of particles in coronal loops.

2. Vlasov-Maxwell Equilibria

We will closely follow the recent work of Mahajan (1989) on Vlasov-Maxwell equilibria of several systems the specific cases of which are Z pinches and tokamaks. A coronal loop will be represented by a cylindrical column of plasma with current density J along the axis of the cylinder and with no gravity. The particle density n, the temperature T, the particle

drift speeds u are in general spatially varying quantities. Here, we allow all spatial variations only in the radial direction. The plasma is embedded in a uniform axial magnetic field B_0. The relevant equations for an equilibrium system are

$$V_r \frac{\partial f_e}{\partial r} - \frac{e}{m_e}\left[\mathbf{E} + \frac{\mathbf{V}}{C} \times (\mathbf{B} + \hat{e}_z B_0)\right] \cdot \frac{\partial f_e}{\partial \mathbf{V}} = 0 \tag{1}$$

$$V_r \frac{\partial f_i}{\partial r} + \frac{e}{m_i}\left[\mathbf{E} + \frac{\mathbf{V}}{C} \times (\mathbf{B} + \hat{e}_z B_0)\right] \cdot \frac{\partial f_i}{\partial \mathbf{V}} = 0 \tag{2}$$

$$\left[\frac{1}{r}\frac{\partial}{\partial r}(rB_\theta)\right] = \frac{4\pi}{C} J_z \tag{3}$$

$$\frac{1}{r}\frac{\partial}{\partial r}(rE_r) = 4\pi\rho \tag{4}$$

$$E_z = 0 = E_\theta = B_r = 0 = B_z,$$

where $f_{i,e}$ are the single particle distribution functions, and $(\mathbf{E}, \mathbf{B})$ are the self-consistent fields. A displaced Maxwellian of the form

$$f_{e,i} = \frac{n_0}{\pi^{3/2} V_{e,i}^3} \exp\left[-(\mathbf{V} - \mathbf{u}_{e,i})^2 / V_{e,i}^2\right] g_{e,i}(r) \tag{5}$$

provides a self-consistent solution of Eqs. (1) to (4). Here n_0 is the ambient density, $V_{e,i} = (2T_{e,i}/m_{e,i})^{1/2}$ and $\mathbf{u}_{e,i}$ are, respectively, the thermal speeds and the drift speeds, and $T_{e,i}$ are the temperatures.

Case I

The entire space dependence lies in the factor $g_{e,i}(r)$. The current and charge densities (J, ρ) are given by

$$\mathbf{J} = -en_0\left[g_e \mathbf{u}_e - g_i \mathbf{u}_i\right] \tag{6}$$

and

$$\rho = -en_0\left[g_e - g_i\right]. \tag{7}$$

The drift speeds are expressed as

$$\mathbf{u}_{e,i} = \hat{e}_z u_z^{e,i} + \hat{e}_\theta u_\theta^{e,i}. \tag{8}$$

Assumption of no charge separation gives

$$g_e = g_i = g \tag{9}$$

and

$$\mathbf{J} = -en_0 \left[\mathbf{u}_e - \mathbf{u}_i\right] g. \tag{9a}$$

Substituting Eqs. (5), (8), and (9) in Eqs. (i) to (4) one gets

$$\frac{1}{g}\frac{dg}{dr} = b \tag{10}$$

$$\frac{1}{r}\frac{\partial}{\partial r}(rb) = -\frac{2g}{\delta_e^2} \tag{11}$$

for

$$u_{e\theta} = u_{i\theta} = 0,$$

where

$$\begin{aligned} b &= \frac{eu_{ez}B_\theta}{CT_e}, \\ \mu &= \frac{u_{iz}}{u_{ez}}, \\ \delta_e^2 &= \frac{2C^2}{\omega_{pe}^2}\frac{V_e^2}{2u_{ez}^2}(1-\mu)^{-1}. \end{aligned} \tag{12}$$

The solutions of Eqs. (10) and (11) are found to be

$$g = \frac{1}{(1 + r^2/4\delta_e^2)^2} \tag{13}$$

and

$$(b\delta_e) = -\frac{r}{\delta_e\,(1 + r^2/4\delta_e^2)}. \tag{14}$$

Thus one obtains a density profile peaked at the axis with a characteristic length scale δ_e which will be estimated in a later section.

Case II

Here, in addition to density, gradient, the spatial variation of temperatures is also allowed. The drift speeds u are still homogeneous. It has been shown (Mahajan 1989) that a series representation for the distribution functions qualifies as a solution of the inhomogeneous Vlasov-Maxwell system, the expansion parameter for the series being (u/v), the ratio of drift and thermal speeds. This is very much appropriate for the considerations in coronal loops as discussed later. Using the smallness of (u/v), we write for the distribution function as

$$f_e = \frac{n_0 g}{\pi^{3/2}\left(V_{e0}\psi_e\right)^3}\exp\left[-\frac{V^2}{V_{e0}^2\psi_e^2}\right] \times\left[1+\frac{2u_e}{V_{e0}}\sum_{n=1}^{\infty}\sum_{m=0}^{\infty}C_{nm}\left(\frac{V_z}{V_{e0}}\right)^n\left(\frac{V}{V_{e0}\psi_e}\right)^{2m}\right], \tag{15}$$

where ψ_e describes the spatial variation of electron temperature and V_{e0} is the thermal speed on the axis ($r=0$). Substituting in Eqs. (1) to (4) and keeping terms only up to (u/V) one finds

$$\frac{1}{g}\frac{dg}{dr} = \left(\frac{3}{2}\beta_\alpha - 1\right)\left[\frac{q_\alpha u_{\alpha 0} B_\theta}{C T_{\alpha 0}}\right] \tag{16}$$

$$\frac{1}{\psi_\alpha}\frac{d\psi_\alpha}{dr} = \frac{\beta_\alpha}{2}\left[\frac{q_\alpha u_{\alpha 0} B_\theta}{C T_{\alpha 0}}\right] \tag{17}$$

which gives

$$g = \psi_\alpha^{3-2/\beta_\alpha} \tag{18}$$

and

$$\frac{1}{r}\frac{\partial}{\partial r}(rb) = \frac{2}{\delta_e^2}\left(\frac{5\beta_\alpha}{2}-1\right)\psi_\alpha^{5-2/\beta} \tag{19}$$

with $C_{10}=1$ and $C_{11}=\beta$. Since we are interested in equilibrium solutions, we assume $\psi_e=\psi_i$ and $\beta_e=\beta_i$, i.e., the electrons and ions have identical temperature profiles. With the wisdom that density variation is generally steeper than temperature variation, one can

take $\beta_e = \beta_i = -\beta$. Substituting for current density J_z as

$$J_z = en_0 g\psi^2 \left(\frac{5\beta}{2} - 1\right)(1+\tau_0)\, u_{e0}$$

we find

$$\frac{1}{r}\frac{d}{dr}\left[r\frac{d}{dr}Q\right] = -\frac{2}{\delta_{\rm eff}^2}e^Q, \tag{20}$$

$$\frac{u_{i0}}{u_{e0}} = -\frac{T_{i0}}{T_{e0}} = -\tau_0 = \mu,$$

$$Q = (5 - 2/\beta)\ln\psi, \tag{21}$$

and

$$\frac{\delta_{\rm eff}}{\delta_e} = \frac{2}{5\beta - 2}.$$

The solution of Eqs. (16), (17), and (19) gives the profile functions as

$$\psi = \left(1 + r^2/4\delta_{\rm eff}^2\right)^{-\frac{2\beta}{5\beta-2}} \tag{22}$$

$$g = \left(1 + r^2/4\delta_{\rm eff}^2\right)^{-\frac{2(3\beta-2)}{5\beta-2}} \tag{23}$$

$$b\delta_{\rm eff} = \left(\frac{5\beta}{2} - 1\right)^{-1} \frac{(r/\delta_{\rm eff})}{(1 + r^2/4\delta_{\rm eff}^2)} \tag{24}$$

with the temperature

$$T \propto \psi^2 = \left(1 + r^2/4\delta_{\rm eff}^2\right)^{-\frac{4\beta}{5\beta-2}}, \tag{25}$$

the current density

$$J \propto g\psi^2 = \left(1 + r^2/4\delta_{\rm eff}^2\right)^{-2}, \tag{26}$$

and the pressure

$$p \propto g\psi^2 = \left(1 + r^2/4\delta_{\rm eff}^2\right)^{-2}. \tag{27}$$

One observes that depending upon the value of β the radial variation can be positive or negative. Thus for $\beta > 2/3$, both density and temperature fall away from the axis, whereas

for $2\beta/3 > 2/5$, the density increases and temperature decreases away from the axis. For $\beta < 2/5$ the temperature increases towards the surface and this is very much reminiscent of cool core and hot sheath type of loops observed by Foukal (1978) and Krieger et al. (1976) and modelled through variational principle in MHD by Krishan (1983, 1985). The other parameter δ_e which characterizes the spatial variations is related to the skin depth. We shall see in a later section that the measure of δ_e, which determines the steepness and extent of the current density profile is commensurate with the requirements laid down by the joule heating of a loop plasma.

Case III

Here, we allow gradients in density and drift speed. It is found that the presence of temperature anisotropy permits a displaced Maxwellian solution of the system where the distribution functions are given by

$$f_{e,i} = \frac{n_0 g(r)}{\pi^{3/2} V_{e,i}^2 V_z^{e,i}} \exp\left[-\frac{V_r^2 + V_\theta^2}{V_{e,i}^2} - \frac{\left(V_z - u_{0z}^{e,i}\phi_{e,i}(r)\right)^2}{\left(V_z^{e,i}\right)^2}\right] \tag{28}$$

and the field equations are

$$b = \frac{1}{\lambda}\frac{\partial \phi}{\partial r} \tag{29}$$

$$\frac{1}{r}\frac{\partial}{\partial r}(rb) = -\frac{2}{\delta_e^2} g\phi \tag{30}$$

and

$$\frac{1}{g}\frac{dg}{dr} = -2\left(\frac{u_{0z}^e}{V_{ez}}\right)^2 \phi \frac{\partial \varphi}{\partial r}, \tag{31}$$

where

$$\lambda = V_e^2 - \frac{V_{z0}^2}{2u_{0ze}^2} = \frac{T_e - T_{ez}}{m_e u_{0ze}^2} = \frac{\Delta T_e}{T_e}\frac{V_e^2}{2u_{0ze}^2}$$

is a measure of the temperature anisotropy. Here, we have taken $\phi_e = \phi_i = \phi$ with $\phi(r=0) = 1$, and $g(r=0) = 1$. Solving Eq. (31) for g in terms of ϕ and substituting it and for b from

Eq. (29) into Eq. (30), one gets

$$\frac{1}{r}\frac{\partial}{\partial r}\left(r\frac{\partial \phi}{\partial r}\right) = -\frac{2\lambda}{\delta_e^2}\phi \exp\left[\left(\frac{u_{0ze}}{V_{ez}}\right)^2\left(\varphi^2-1\right)\right] \tag{32}$$

and

$$g = \exp\left[\left(\frac{u_{0ze}}{V_{ze}}\right)^2\left(\varphi^2-1\right)\right]. \tag{33}$$

Equation (32) has been solved numerically and here we will reproduce some of the figures given in Mahajan (1989), since the spatial behavior of the density, the magnetic field, and the current density is essentially a function of the dimensionless parameter λ.

3. Coronal Loops

Coronal loop, a bipolar structure is characterized by an electron density $n_0 \sim 10^{10}$–10^{12}cm^{-3}; a temperature varying from a few tens of thousands to a couple of million degrees Kelvin, a length of $10^9 - 10^{10}$cm and a radius of $10^8 - 10^9$cm with an axial magnetic fields of a few Gauss. The current flows essentially along the axis of the cylindrical plasma column and produces an azimuthal component B_θ of the magnetic field. Observations in EUV have shown that loops of different temperatures are coaxial and this has led to the identification of cool core and hot sheath type of loops, Foukal (1978), Krishan (1983, 1985). The x-ray observations further reinforce the inhomogeneous nature of the underlying heating mechanisms. Resonance absorption of surface MHD waves as well as the joule dissipation of high density current sheets in addition to the ubiquitous mini magnetic reconnections are some of the favored candidates for heating of the solar corona in general and coronal loops in particular, Hollweg (1981). Here, we find that the exact solution of a Vlasov-Maxwell system naturally admits the peaked spatial profiles of current density and magnetic field and we believe it is this equilibrium configuration when disturbed gives rise to sporadic phenomena of flaring, acceleration, and heating. It has been shown by Rosner et al. (1978) and Hollweg

(1981) that for the joule dissipation to provide enough heating to balance the radiation losses for the typical conditions of electron density, magnetic field, and temperature, the current sheath must have a thickness of a few hundred to a thousand cms and anomalous instead of the collisional resistivity must be operative. The latter gives us a clue to the relative electron-ion drift velocity that must exist to excite ion-acoustic turbulence which may be responsible for anomalous resistivity. The typical parameters in this scenario are chosen to be, Hollweg (1981)

$$\begin{aligned}
\text{electron density in the sheath } n &= 10^9\text{cm}^{-3}, \\
\text{electron temperature in the sheath } T_e &= 2.5 \times 10^7\text{K}, \\
\text{electron thermal speed } V_e &= 2.7 \times 10^9\text{cm/sec}, \\
\text{electron drift velocity } u_e > \text{sound speed} &= 4.5 \times 10^7\text{cm/sec},
\end{aligned}$$

the magnetic field B_θ produced by the current density J_z is 10 Gauss, and the thickness (ΔR) of the current sheet turns out to be $\sim 10^3$cm. We recall from the previous section that δ_e emerges to be the characteristic length scale in the solutions of Vlasov-Maxwell system. Let us estimate it

$$\begin{aligned}
\delta_e &= \frac{c}{\omega_{pe}} \frac{V_e}{u_e} \left(1 + \frac{T_i}{T_e}\right)^{-1/2} \\
&= 1.04 \times 10^3\text{cm for } T_e \gg T_i \\
&= 0.97 \times 10^3\text{cm for } T_e = 9T_i.
\end{aligned}$$

Thus we find that current profile of small widths are outcomes of the exact solutions of the Vlasov-Maxwell system. Here, we present a few examples of spatial variations of plasma parameters. The variation of density g and magnetic field b profile factors for Case I where only the density is space dependent, is given by Eqs. (13) and (14) and is shown in Figs. 1

and 2. A sharp fall in density away from the axis is obtained. This is reminiscent of the condensations often observed at the axis of a loop. The current density accordingly is found to be maximum on the axis. The spatial profiles for Case II allowing temperature variation are given by Eqs. (23), (24), and (25) and are shown in Figs. 3, 4, and 5 for three values of the parameter β. In this case the temperature increase [Eq. (25)] away from the axis is found for $\beta < 2/5$. Case III gives very interesting profiles where the current density (gu) appears in the form of multisheaths (Fig. 6) for large value of the anisotropy parameter; the corresponding density profile (Fig. 7) is almost flat. These profiles are reproduced from Mahajan (1989). Since all functions as well as the variables are expressed in dimensionless forms, we only need to provide appropriate normalization. For coronal loops, the anisotropy parameter

$$\begin{aligned} \lambda &= \frac{\Delta T_e}{T_e}\frac{V_e^2}{2u_{e0}^2} \\ &= 1.8 \times 10^3 \frac{\Delta T_e}{T_e}. \end{aligned}$$

Thus for $\lambda = 5$ one finds

$$\frac{\Delta T_e}{T_e} = 2.7 \times 10^{-3},$$

which is reasonably small.

4. Conclusion

A Vlasov-Maxwell description of coronal loop plasma admits a variety of equilibrium spatial profiles of mass density, current density, the temperature and the magnetic field depending upon the type of inhomogeneities allowed. The profiles vary from being flat to spiky and do resemble the ones derived from EUV and x-ray coronal observations. Especially the multisheath current profiles derived here complement the magnetohydrodynamic study of current sheet formation.

Acknowledgement

This work was supported by U. S. Dept. of Energy Contract No. DE-FG05-80ET-53088.

References

Foukal, P. V., 1978, Astrophys. J. **223**, 1046.

Hollweg, J. V., 1981, "Solar Active Regions," edited by Frank Q. Orrall, p. 277. Colorado Associated University Press.

Hood, A. W. and Priest, E. R.: 1979, Astron. Astrophys. **77**, 233.

Karpen, J. T., Antiochos, S. K., and De Vove, C. R., 1990, Astrophysical Journal Letters.

Krieger, A. S., de Feiter, L. D., and Vaiana, G. S.: 1976, Solar Phys. **47**, 117.

Krishan, V., 1983, Solar Phys. **88**, 155.

Krishan, V., 1985, Solar Phys. **97**, 183.

Krishan, V.: Berger, M. and Priest, E. R.: 1988. "Solar and Stellar Coronal Structures and Dynamics," Ed.: Richard C. Altrock.

Low, B. C., 1987, Astrophys. J. **323**, 358.

Low, B. C. and Wolfson, R., 1988 Astrophys. J. **324**, 574.

Mahajan, S. M., 1989. Phys. Fluids B1 **1**, 43.

Parker, E. N., 1983, Astrophys. J., **264**, 635.

Parker, E. N. 1987, Astrophys. J. **318**, 876.

Priest, E. R., 1981, "Solar Flare Magnetohydrodynamics," p. 2 and 139. Ed.: E. R. Priest, Gordon and Breach Science Publishers.

Rosner, R. et al., 1978, Astrophys. J. **222**, 317.

Tsinganos, K. C., 1982, Astrophys. J. **259**, 820.

Vaiana, G. S. and Rosner, R.: 1978 Ann. Rev. Astron. Astrophys. **16**, 393.

Van Ballegooijen, A. A., 1985, Astrophys. J. **298**, 421.

Van Ballegooijen, A. A., 1986, Astrophys. J. **311**, 1001.

Figure Captions

1. Variation of density profile function g vs. $x = r/\delta e$ for Case I [Eq. (13)].

2. Variation of magnetic field profile function $(b\delta e)$ vs. x for Case I [Eq. (14)].

3. a) Variation of temperature profile function ψ^2 vs. x for $\beta = 0.5$ [Eq. (25)].
   b,c) Variation of $(b\delta e)$ and g vs. x for $\beta = 0.5$ [Eqs. (24) and (23)].

4. Variation of ψ^2, $(b\delta e)$ and g vs. x for $\beta = 0.8$.

5. Variation of ψ^2, $(b\delta e)$ and g vs. x for $\beta = 0.2$.

6. Variation of current profile function (gu_e) vs. x showing formation of multisheaths for large value of anisotropy parameter λ [from Mahajan (1989)].

7. Variation of density profile function g vs. x for several values of the anisotropy parameter λ [from Mahajan (1989)].

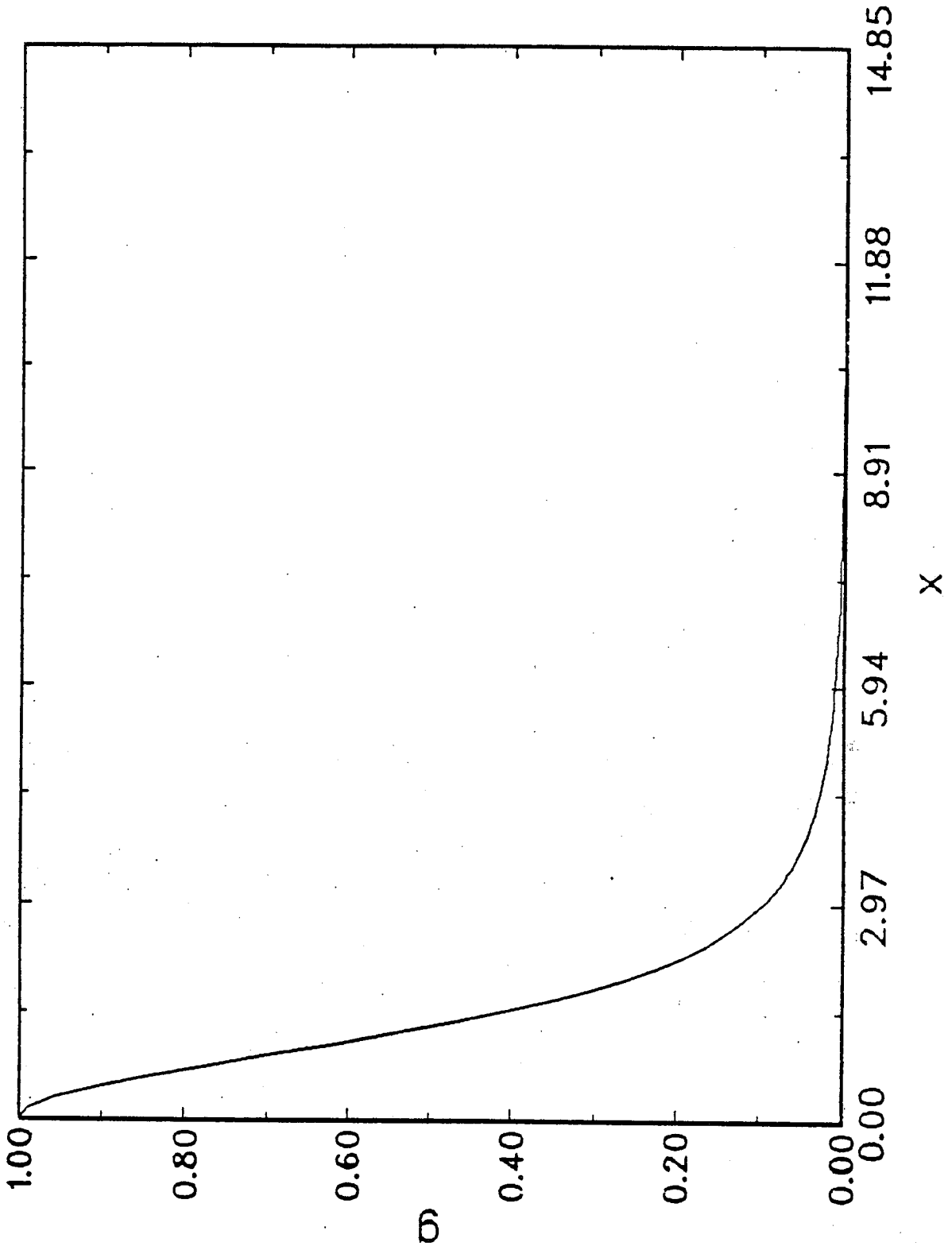

Figure 1

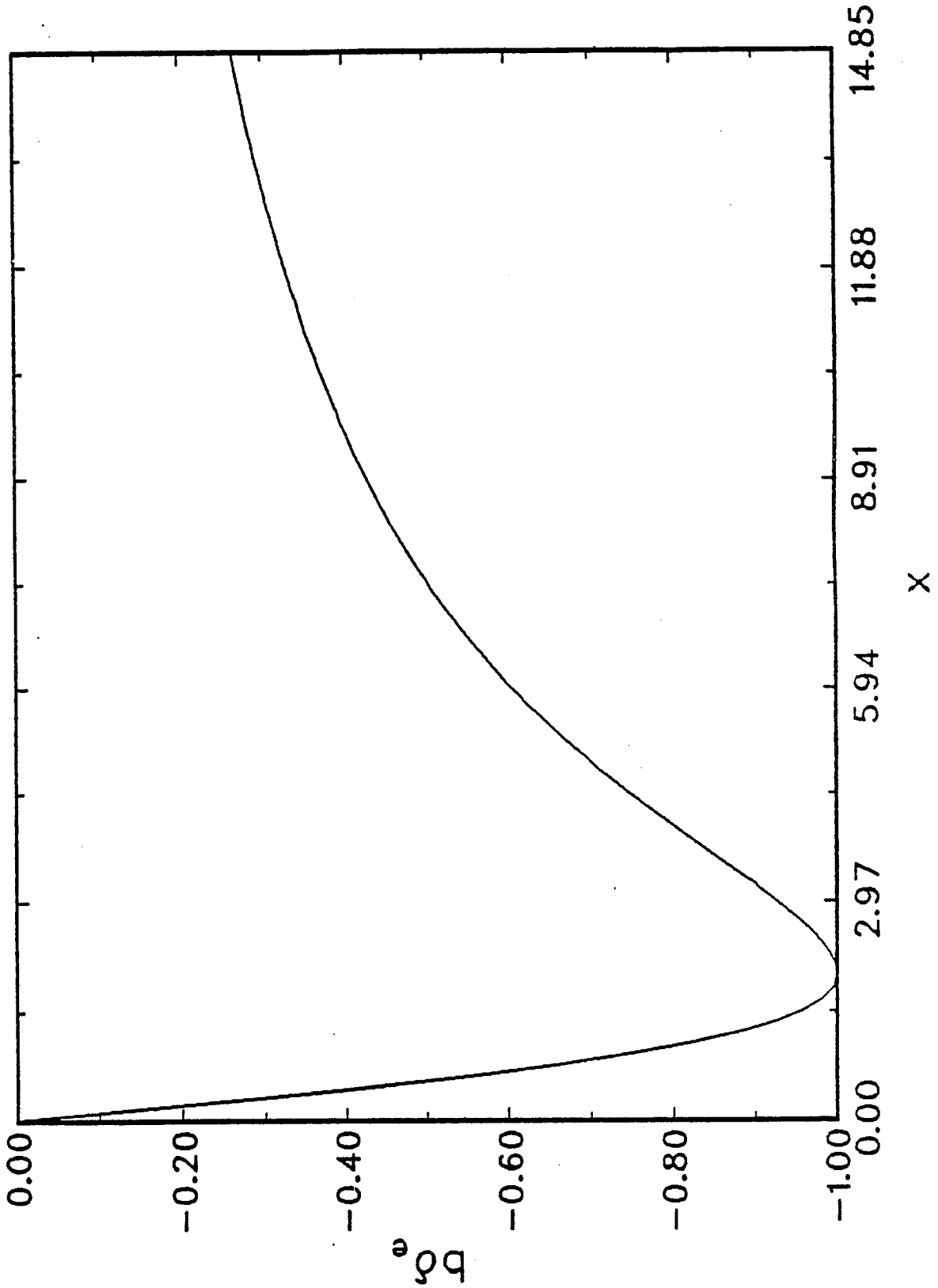

Figure 2

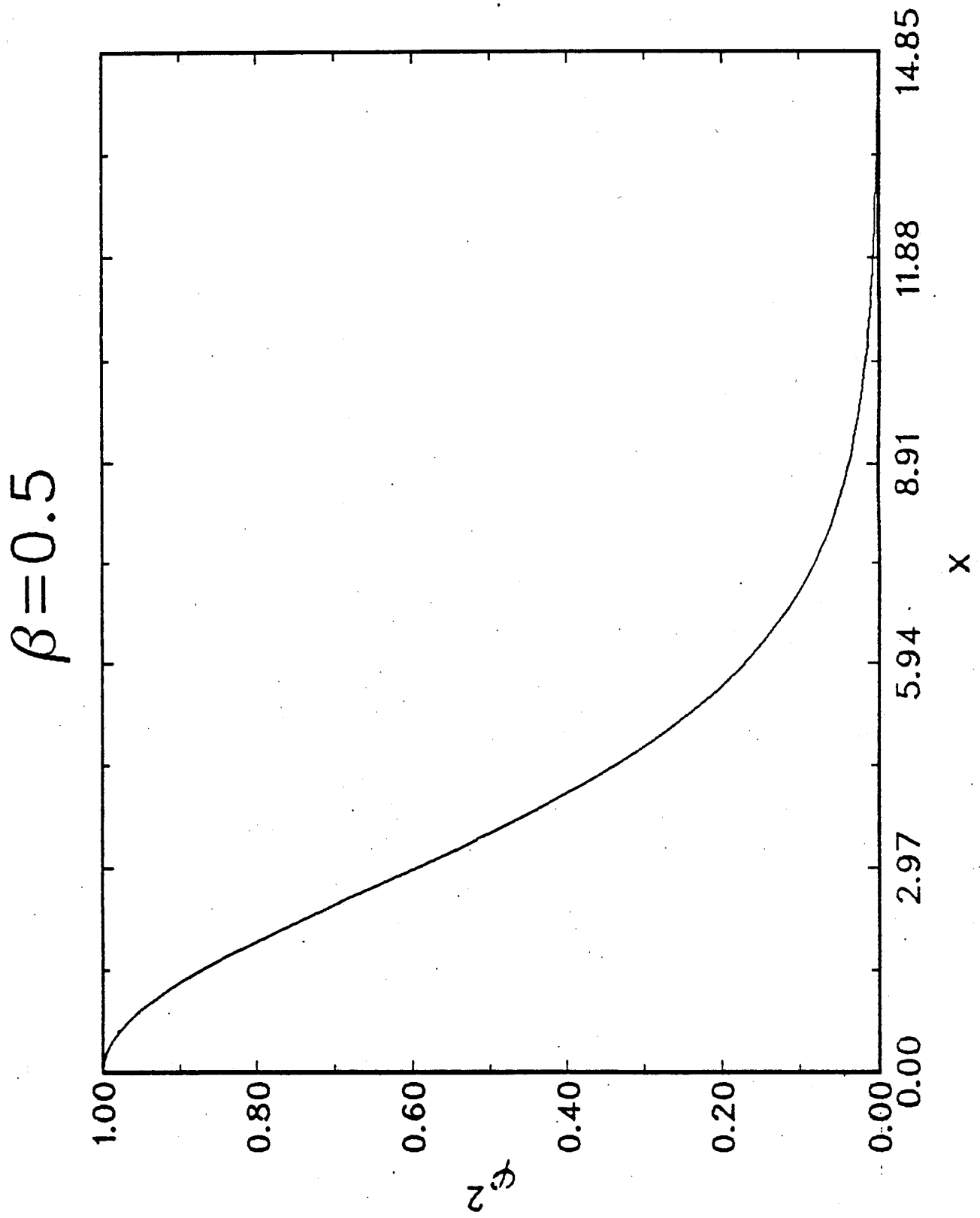

Figure 3a

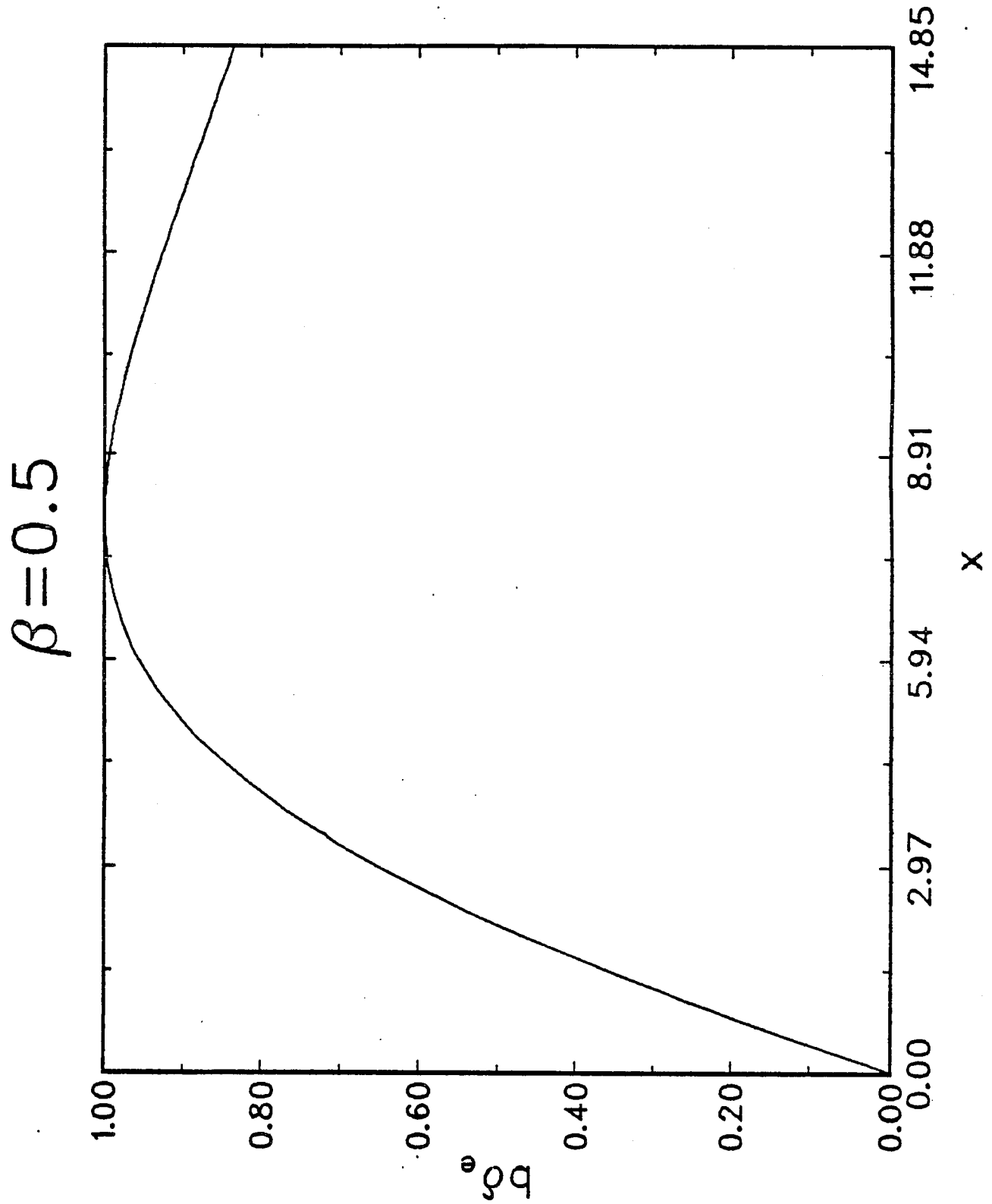

Figure 3b

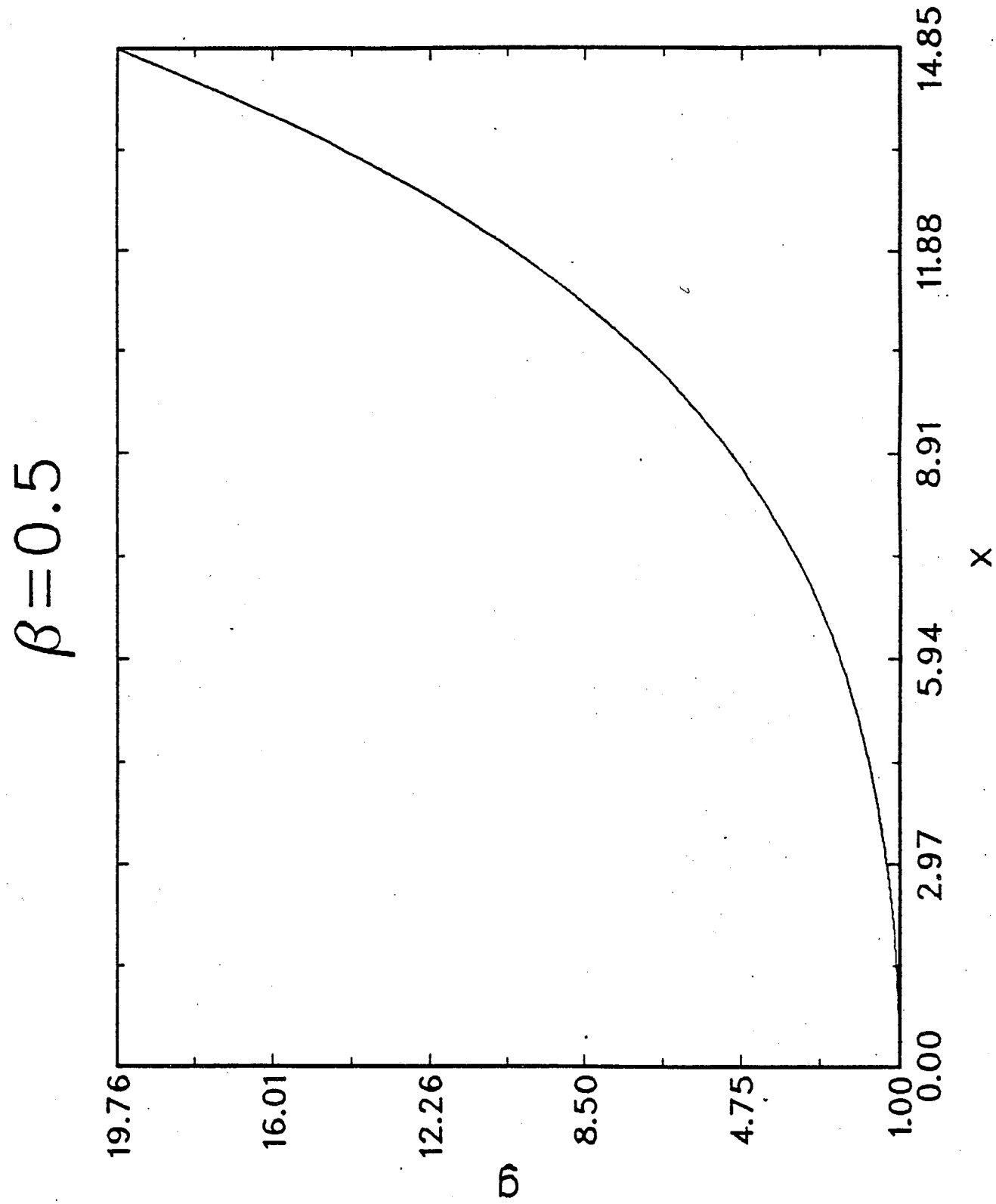

Figure 3c

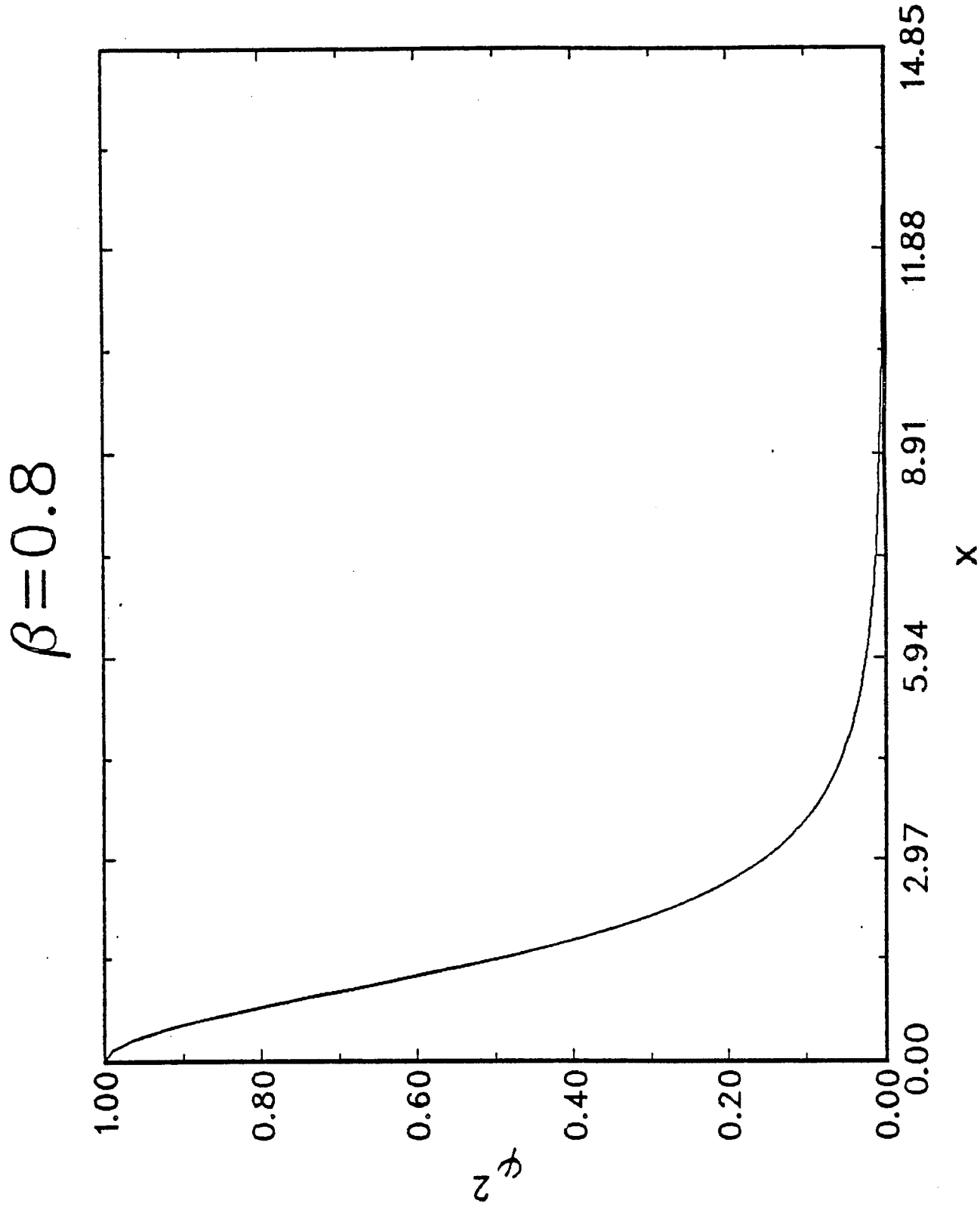

Figure 4a

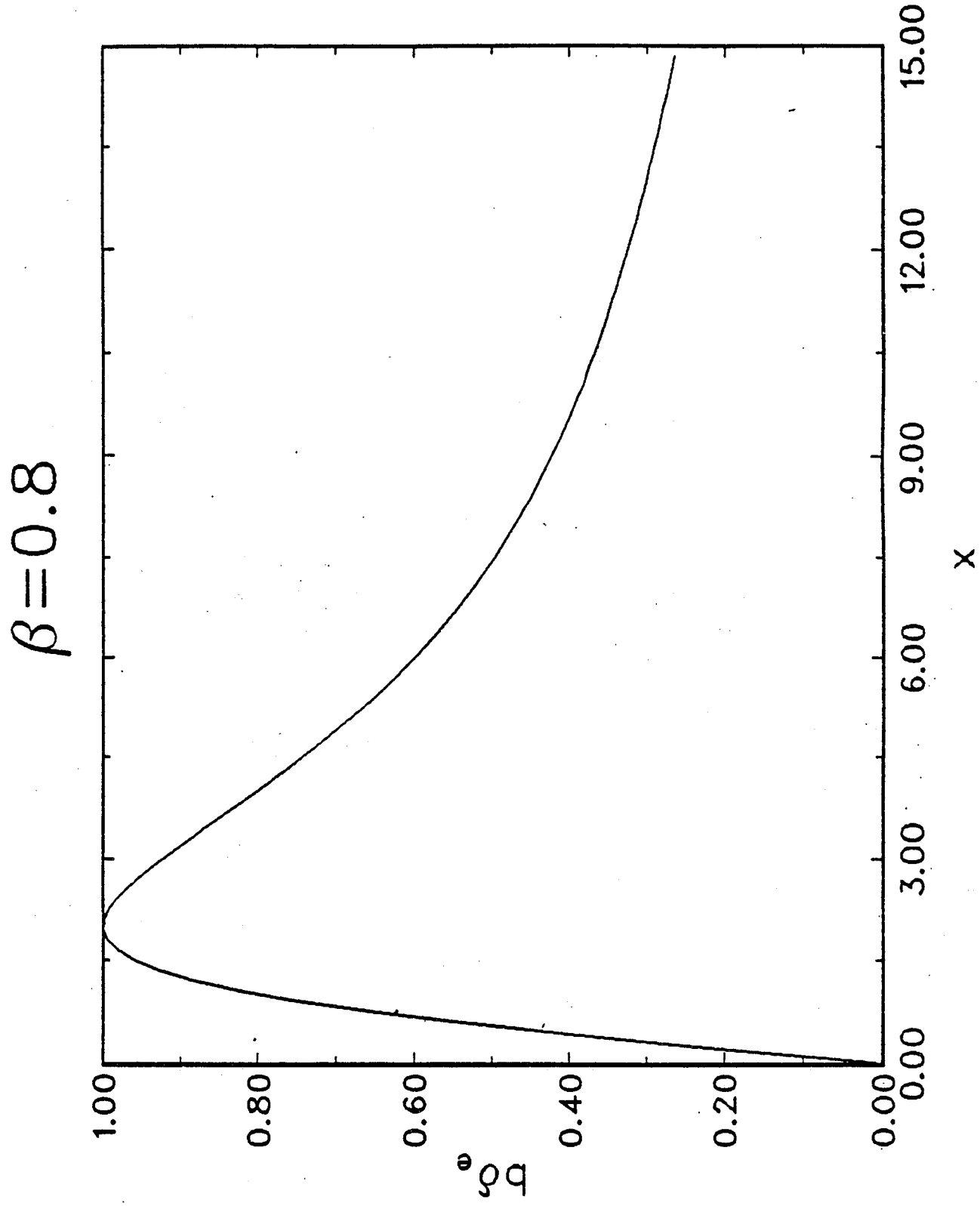

Figure 4b

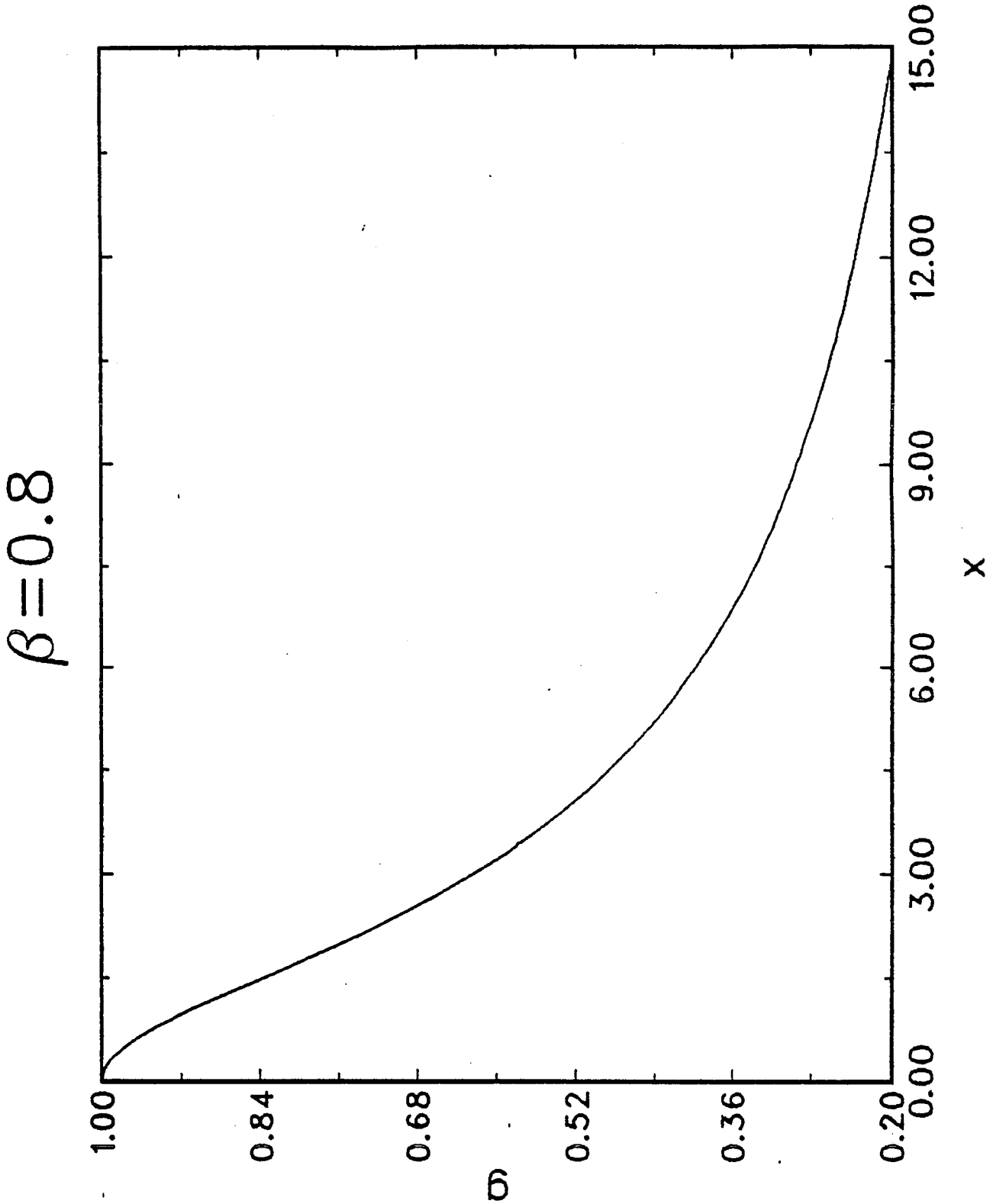

Figure 4c

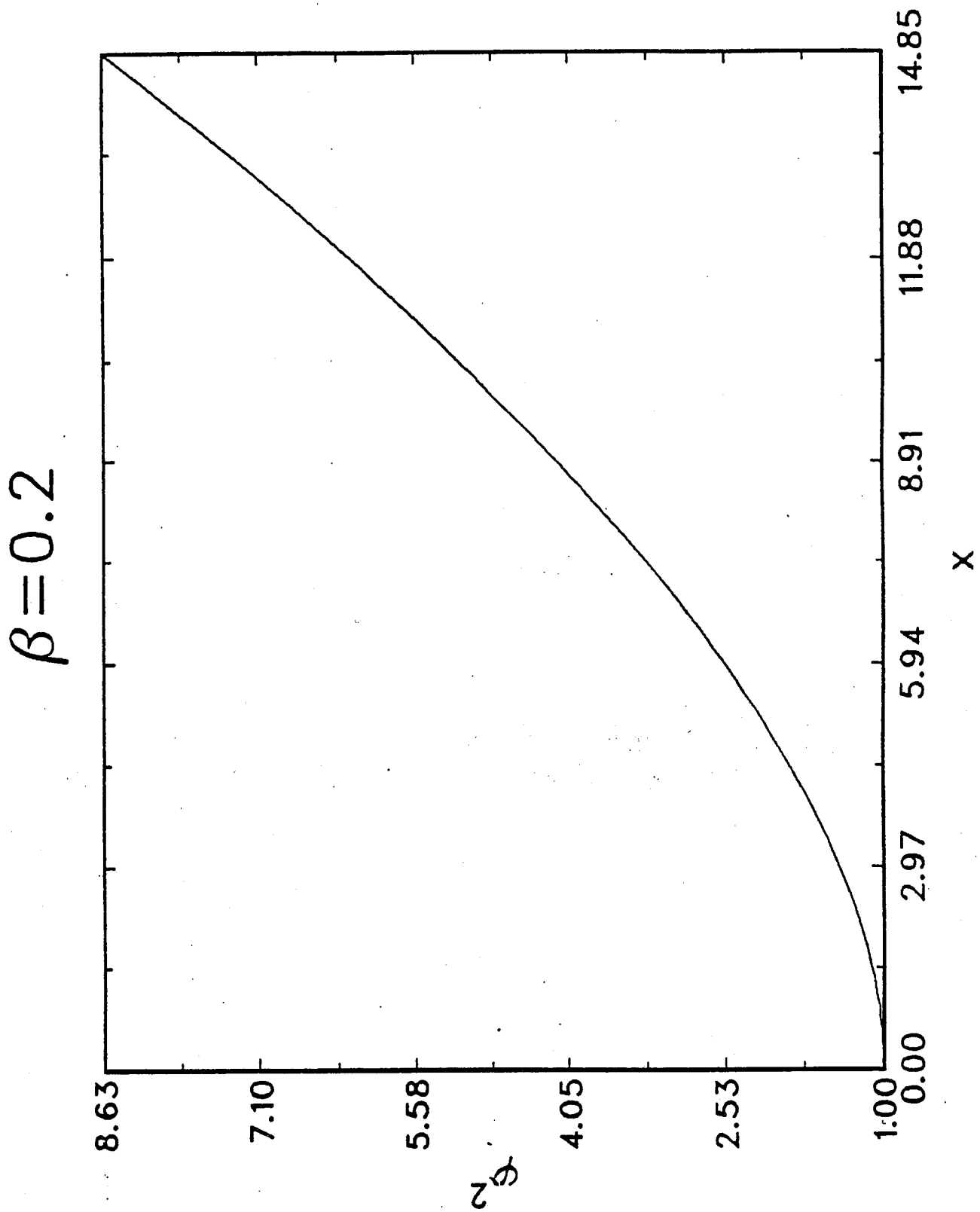

Figure 5a

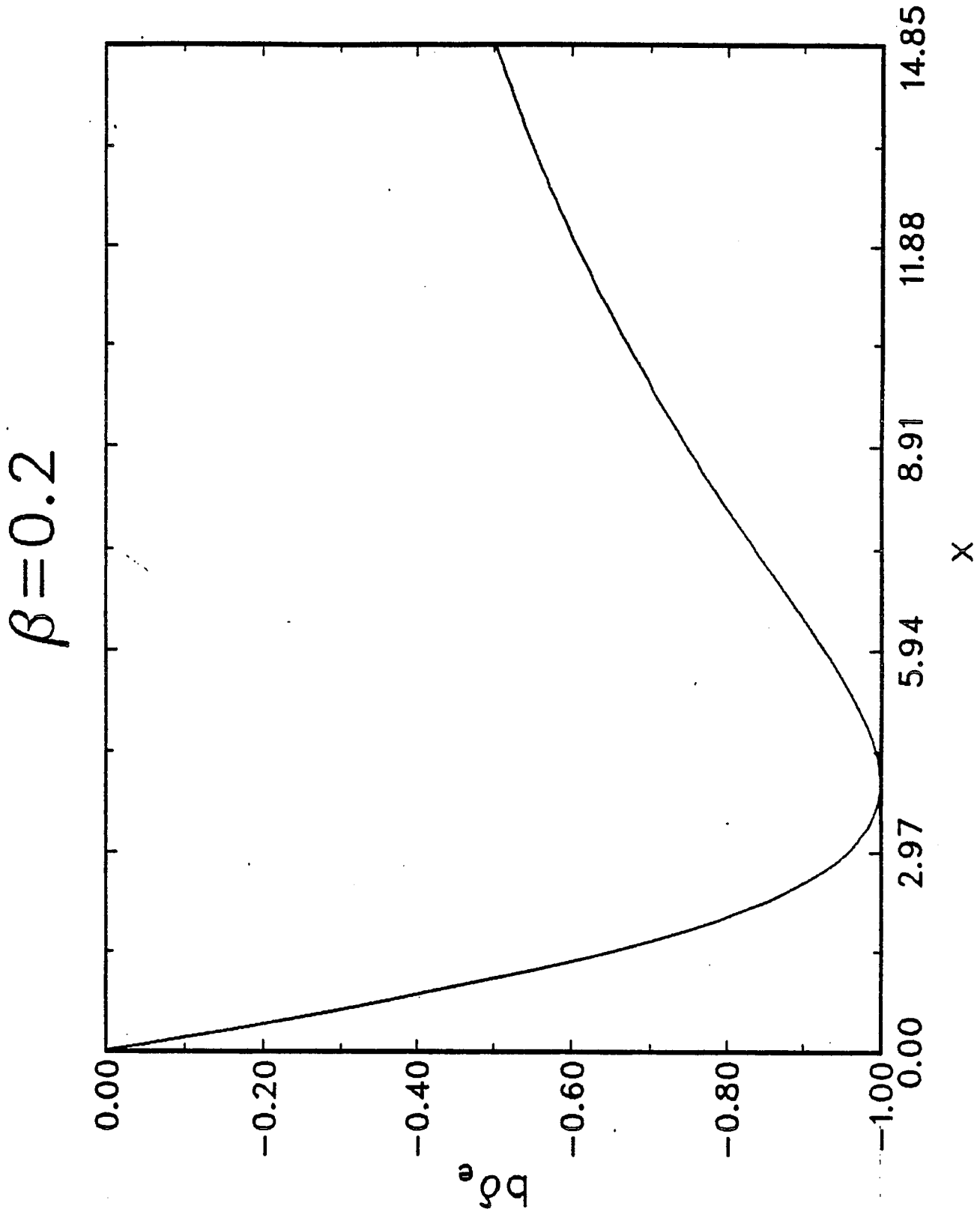

Figure 5b

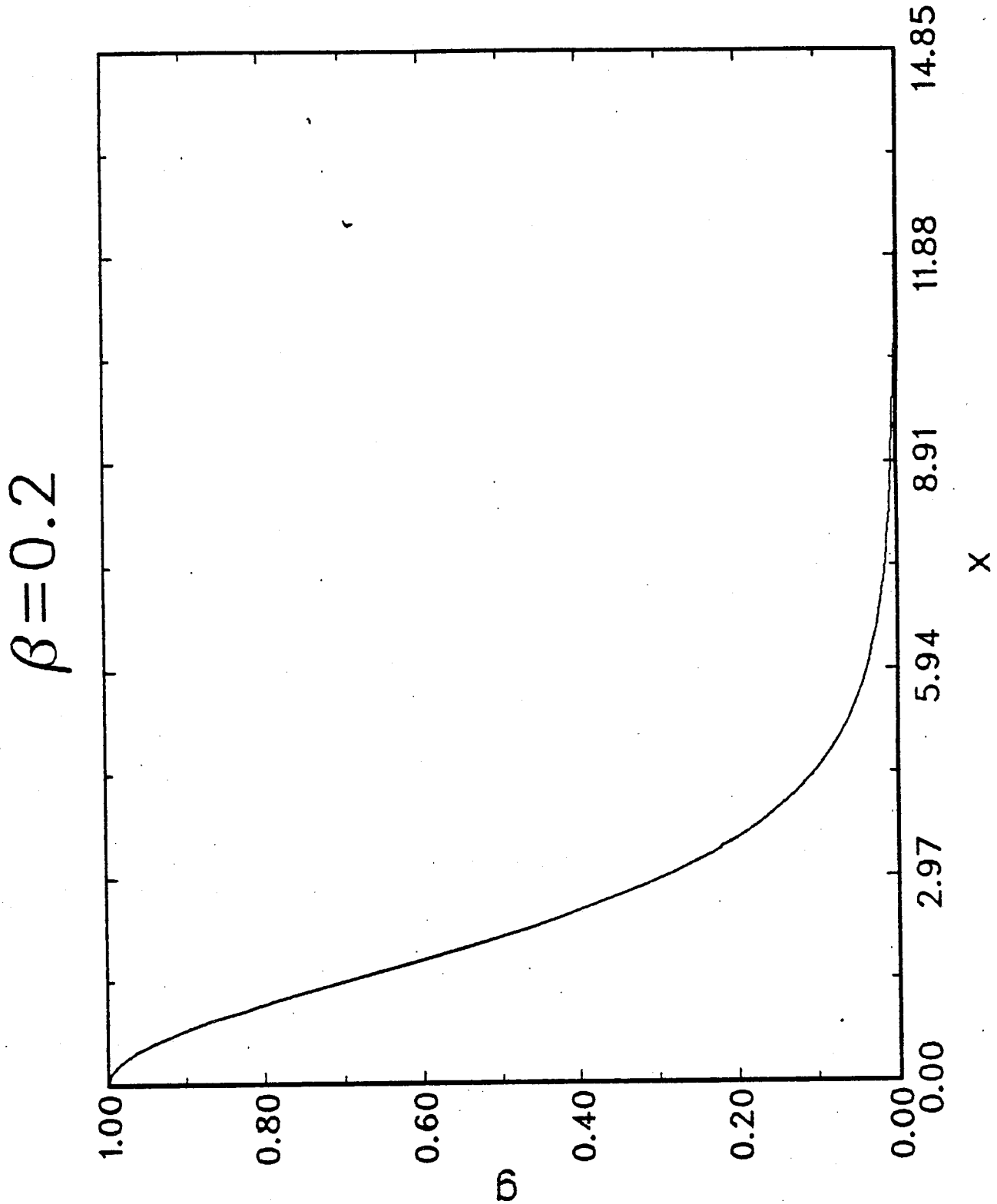

Figure 5c

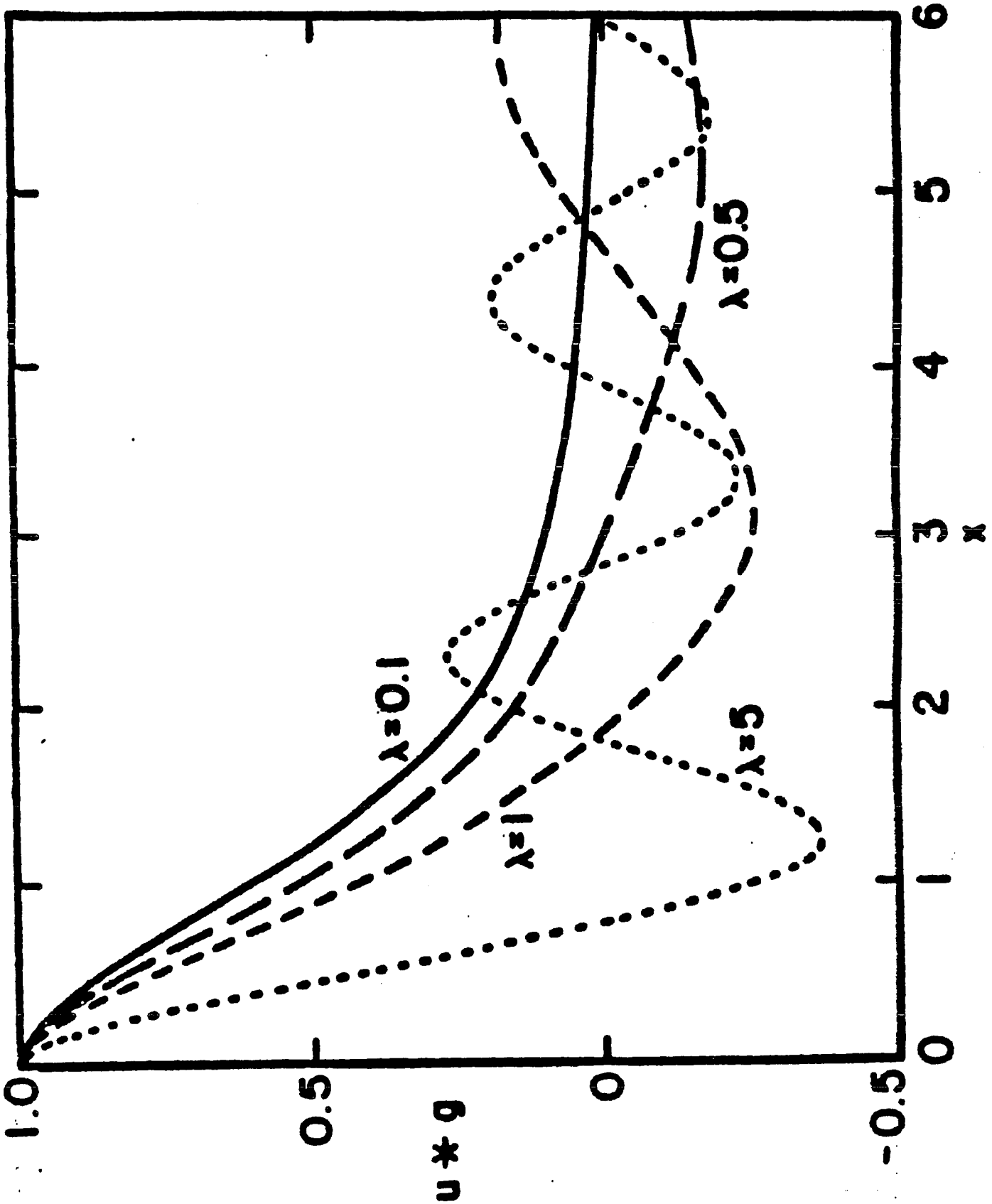

Figure 6

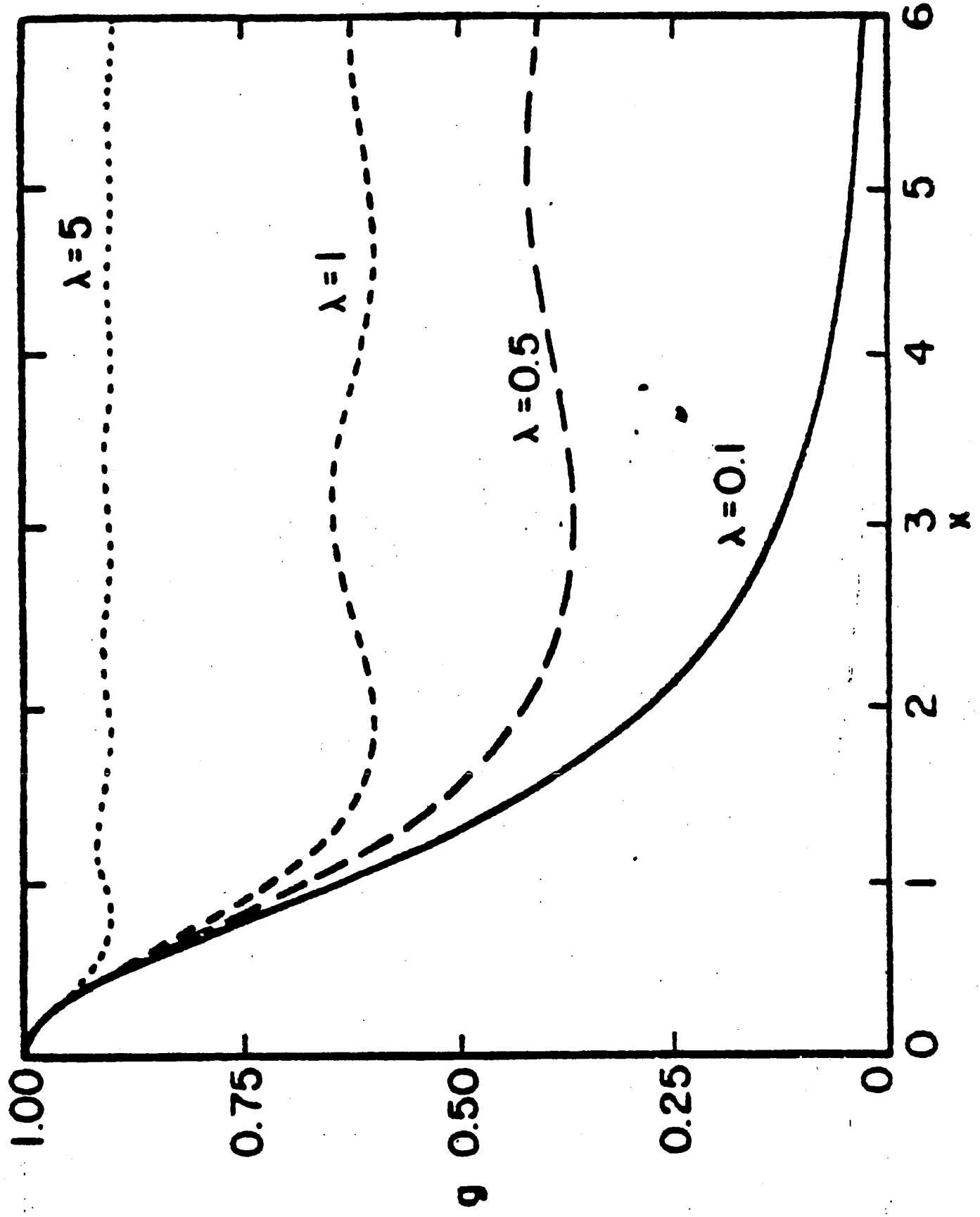

Figure 7